PROCEEDINGS OF SCIENCE

Status of non-supersymmetric models with GAMBIT

Pat Scott* **for the GAMBIT Collaboration**
School of Mathematics & Physics, The University of Queensland, St Lucia, Brisbane QLD 4072, Australia
E-mail: pat.scott@uq.edu.au

I briefly review the latest analyses of non-supersymmetric models from the GAMBIT global fitting project, covering axions, axion-like particles and scalar, vector and fermionic Higgs portal models stabilised by either a $\mathbb{Z}_2$ or $\mathbb{Z}_3$ discrete symmetry. These results incorporate various combinations of constraints from the LHC, direct and indirect searches for dark matter, dedicated axion experiments, vacuum stability and the observed relic density of dark matter (applied as either an upper limit or a strict requirement). They also include the impacts of theoretical uncertainties ranging from the temperature dependence of the QCD axion mass to nuclear matrix elements, Standard Model parameters and astrophysical halo modelling.

ALPS 2019: An Alpine LHC Physics Summit
April 22 - 27, 2019
Obergurgl, Austria

*Speaker.

PoS(ALPS2019)027

The Global and Modular Beyond-the-Standard Model (BSM) Inference Tool (GAMBIT) [1] is a framework for carrying out global fits of BSM theories. It includes modules for predicting and comparing dark matter [2], collider [3], flavour [4] and precision [5] observables with experimental results, extensive sampling and statistical routines [6], and interfaces to most of the other leading public BSM theory and phenomenology codes. It has so far led to a series of results for supersymmetric models [7–9] (see also [10]), as well as the most comprehensive analyses to date on a number of other models ranging from axions to axion-like particles (ALPS; [11]), scalar singlet dark matter [12, 13] and generalised gauge-singlet Higgs portal dark matter models [14].

The viable parameter space of ALPS (Fig. 1 left) is constrained at high photon couplings by observations of supernovae (*SN1987A*), transparency of the extragalactic medium at gamma-ray energies (*HESS*), axion helioscopes (*CAST '17*), and evolution of horizontal branch stars (and to a lesser extent, red giants; *R parameter*). For a limited range of masses, axion haloscopes provide sufficiently stringent constraints to not only constrain ALPs, but also the region of parameter space in which QCD axion models are otherwise viable. These constraints however become weaker for models where QCD axions can provide only a fraction of the observed DM density. Accounting self-consistently for the experimental constraints alongside the implications of individual models' cosmological abundances, a Bayesian global analysis (Fig. 1 right) reveals a preferred QCD axion mass window of $10^{-7}\,\mathrm{eV} \lesssim m_a \lesssim 10^{-2}\,\mathrm{eV}$.

The allowed parameter space of scalar singlet dark matter (Fig. 2) splits into a low-mass region at $m_S \leq m_h/2$ dominated by the resonance associated with s-channel annihilation via a Higgs boson,

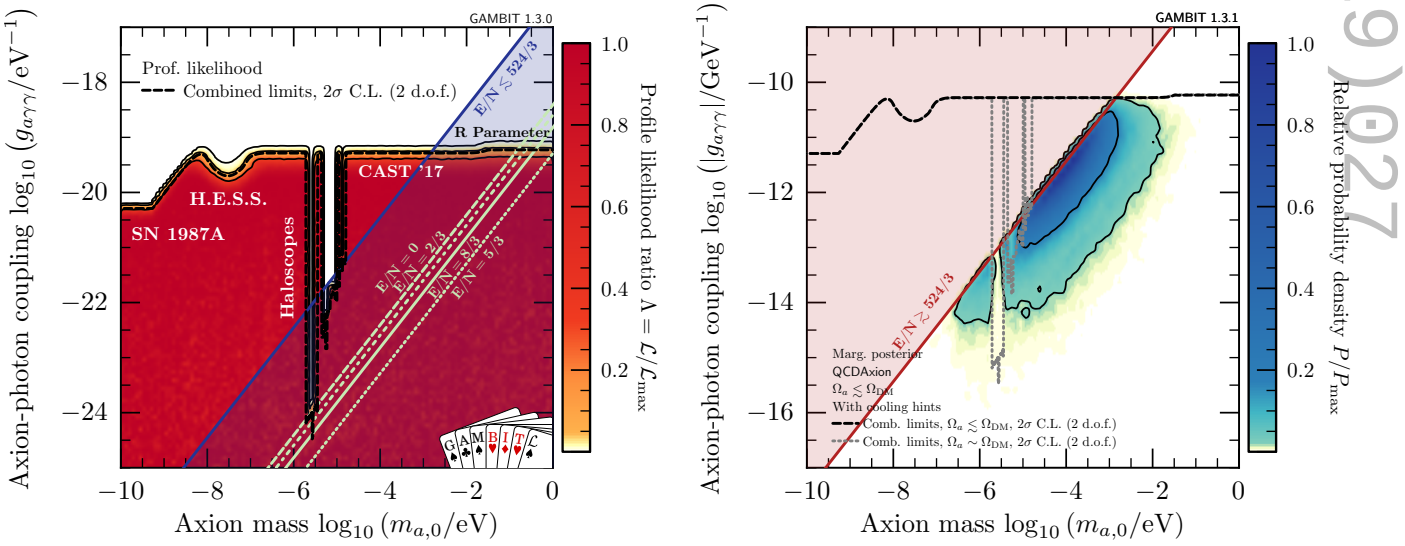

Figure 1: Constraints on axion-like particle (ALP; left) and QCD axion (right) models from global fits with GAMBIT. Black contours indicate 1σ and 2σ confidence/credible regions of the respective fits, whereas dashed lines in the right panel indicate the combined 2σ ALP limits in the case where ALPs make up all (black) or none (grey) of dark matter. Leading constraints on ALPs in different parts of the parameter space are indicated with annotations in the left panel. The theoretically viable region for QCD axion models is shaded in blue in the left panel, whereas the theoretically inaccessible region is shown shaded in red in the right panel. From Ref. [11].

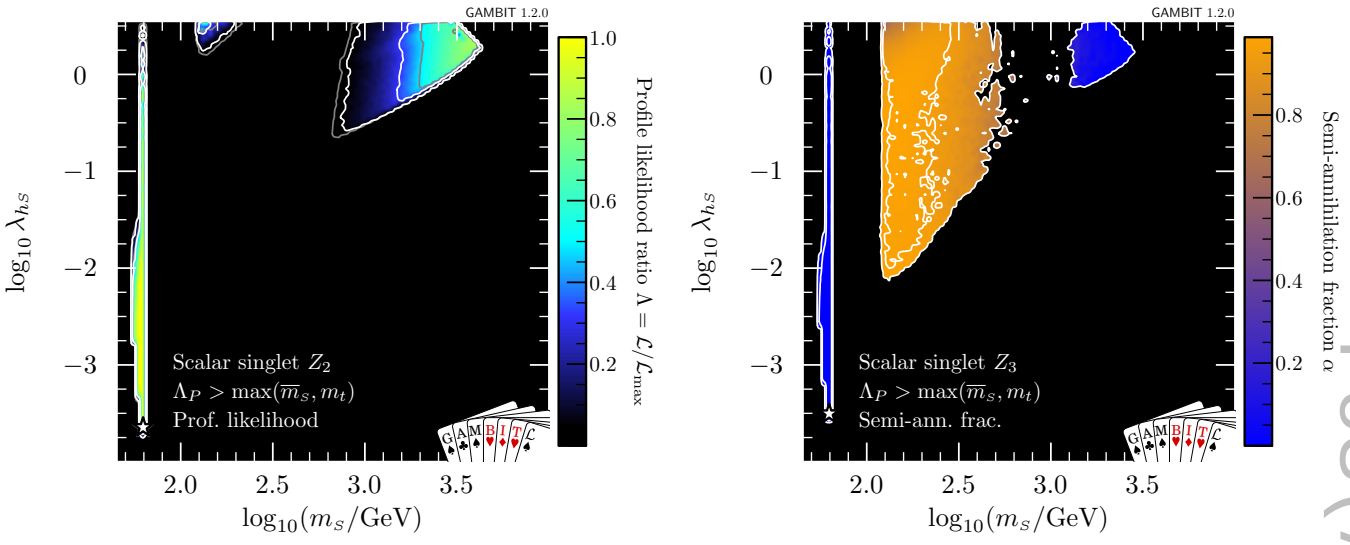

Figure 2: Constraints on scalar singlet dark matter stabilised by a $\mathbb{Z}_2$ (left) or $\mathbb{Z}_3$ (right) symmetry from global fits with GAMBIT. White contours indicate 1σ and 2σ confidence regions of the respective fits, and white stars indicate the overall best-fit points. Shading in the left panel indicates the profiled likelihood at each mass and coupling, whereas shading in the right panel indicates the degree to which the relic density of the singlet is determined by semi-annihilation processes in the best-fit model at each mass-coupling combination, within the overall 2σ likelihood contours. Grey contours in the left panel indicate the impact of using 2017 XENON1T results [15] in the fit, instead of the 2018 results [16] used in the main fit. Λ_P annotations refer to the fact that the model was only required to remain perturbative up to the highest mass scale in the theory (rather than to the scale of second minimum of the Higgs potential, or the unification scale). From Ref. [13].

and a high-mass region constrained predominantly by direct detection and the thermal abundance of dark matter. In models where the scalar singlet respects a $\mathbb{Z}_2$ symmetry, the singlet is a self-conjugate particle and has its relic density set exclusively by self-annihilation. If the stabilising symmetry is instead $\mathbb{Z}_3$, both singlet S and anti-singlet S^* dark matter exist in equal numbers, and the Lagrangian includes an additional cubic scalar self-interaction. This leads to additional semi-annihilation processes $SS \to S^*h$ and $S^*S^* \to Sh$, which further deplete the relic density, allowing a broader part of the high-mass region to evade constraints from direct detection. This is shown in Fig. 2 (right), where the allowed regions of the $\mathbb{Z}_3$-symmetric variant are coloured in terms of the semi-annihilation fraction α, defined as

$$\alpha = \frac{1}{2}\frac{\langle\sigma v_{\mathrm{rel}}\rangle_{SS\to hS}}{\langle\sigma v_{\mathrm{rel}}\rangle + \frac{1}{2}\langle\sigma v_{\mathrm{rel}}\rangle_{SS\to hS}}, \tag{1}$$

with $\langle\sigma v_{\mathrm{rel}}\rangle_{SS\to hS}$ the thermally-averaged semi-annihilation cross-section and $\langle\sigma v_{\mathrm{rel}}\rangle$ the corresponding value for pure annihilations.

However, if one requires the scalar singlet to fully stabilise the electroweak vacuum, the two variants are driven to slightly different parts of parameter space [13]. With a $\mathbb{Z}_2$ symmetry, the singlet can still satisfy all constraints, and shows a strong preference for a mass of $\sim 2\,\mathrm{TeV}$ and a nuclear scattering cross-section of the order of $10^{-45}\,\mathrm{cm}^2$, consistent with the latest results of

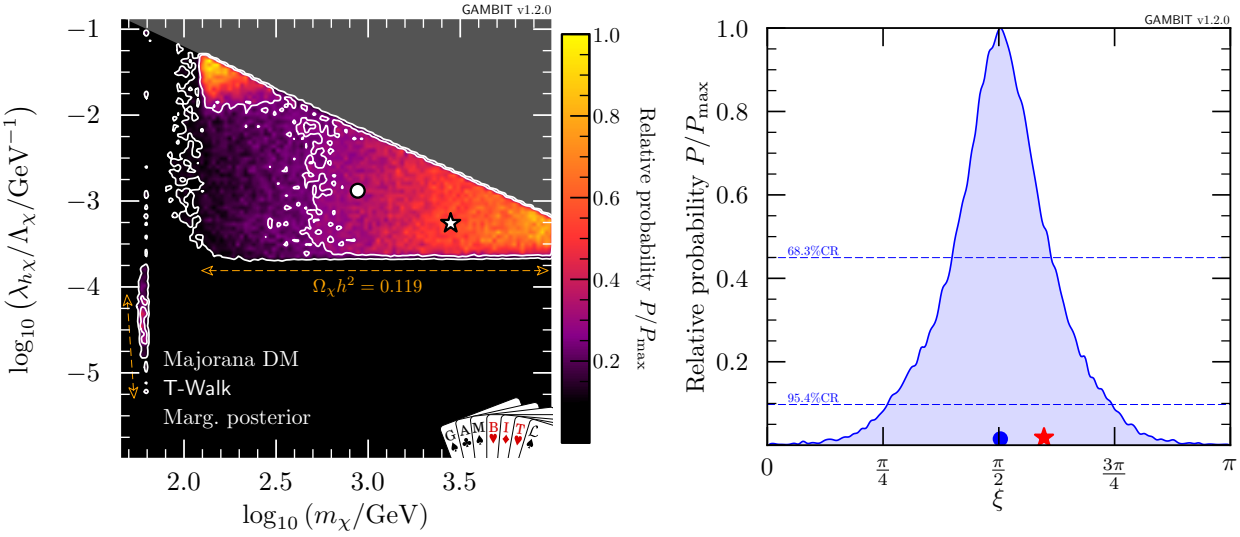

Figure 3: Constraints on Majorana fermion singlet dark matter from global fits with GAMBIT. The left panel shows the posterior probability density in terms of the dark matter mass and portal coupling strength. The right panel shows the relative probability of different CP mixing angles for the portal interaction. $\xi = 0, \pi$ corresponds to a pure CP-even coupling; $\xi = \frac{\pi}{2}$ is a purely CP-odd Higgs portal. In the left panel, the edge of the allowed parameter space where the fermion is all of the observed dark matter is indicated with orange annotations, the grey region corresponds to the parameter region where the fermionic Higgs portal effective field theory breaks down, and "T-Walk" is the sampler [6] used to traverse the parameter space. In both panels, the best fit is indicated by a star, and the posterior mean by a bullet. From Ref. [14]; fits to Dirac fermion and vector singlet Higgs portal models can also be found in Ref. [14].

XENON1T [16] (and indeed, consistent with the weak excess in their data). With a $\mathbb{Z}_3$ symmetry however, the region in which the singlet stabilises the vacuum is strongly in tension with the XENON1T limit. The $\mathbb{Z}_3$ model is thus excluded as a simultaneous explanation for (any fraction of) dark matter and the stability of our vacuum at more than 98% confidence.

Dirac fermion, Majorana fermion and vector singlet Higgs portal dark matter models show broadly similar phenomenology to their scalar equivalent (Fig. 3 left), with a low-mass region below the Higgs resonance consistent with all constraints, and a high-mass region constrained mainly by the relic density and direct detection. In addition to the usual CP-conserving interaction with the Higgs, the fermionic variants also possess an additional CP-violating portal coupling. Because the CP-violating coupling leads to a momentum-suppressed nuclear scattering cross-section but an unsuppressed annihilation cross-section, in much of the high-mass region, the constraints imposed by direct detection can be avoided only by enhancing the CP-violating coupling at the expense of the CP-even one. This can be seen in the moderate preference for higher masses or higher couplings in the high-mass region of the left panel of Fig. 3, where this fine-tuning is not required in order to avoid direct detection. Bayesian model comparison of the general CP-violating theory with a pure CP-conserving version (where the coefficient of the CP-violating term is exactly zero, implying a mixing angle of $\xi = 0$ or $\xi = \pi$) indicates a preference for the CP-violating theory at the level of approximately 100:1 (Fig. 3 right).

Acknowledgments

I am supported by STFC (ST/K00414X/1, ST/P000762/1, ST/L00044X/1), and thank my collaborators in GAMBIT for their extensive contributions to the results discussed here.

References

[1] GAMBIT Collaboration: P. Athron, C. Balázs, *et. al.*, *GAMBIT: The Global and Modular Beyond-the-Standard-Model Inference Tool*, *Eur. Phys. J. C* **77** (2017) 784, [arXiv:1705.07908].

[2] GAMBIT Dark Matter Workgroup: T. Bringmann, J. Conrad, *et. al.*, *DarkBit: A GAMBIT module for computing dark matter observables and likelihoods*, *Eur. Phys. J. C* **77** (2017) 831, [arXiv:1705.07920].

[3] GAMBIT Collider Workgroup: C. Balázs, A. Buckley, *et. al.*, *ColliderBit: a GAMBIT module for the calculation of high-energy collider observables and likelihoods*, *Eur. Phys. J. C* **77** (2017) 795, [arXiv:1705.07919].

[4] GAMBIT Flavour Workgroup: F. U. Bernlochner, M. Chrząszcz, *et. al.*, *FlavBit: A GAMBIT module for computing flavour observables and likelihoods*, *Eur. Phys. J. C* **77** (2017) 786, [arXiv:1705.07933].

[5] GAMBIT Models Workgroup: P. Athron, C. Balázs, *et. al.*, *SpecBit, DecayBit and PrecisionBit: GAMBIT modules for computing mass spectra, particle decay rates and precision observables*, *Eur. Phys. J. C* **78** (2018) 22, [arXiv:1705.07936].

[6] GAMBIT Scanner Workgroup: G. D. Martinez, J. McKay, *et. al.*, *Comparison of statistical sampling methods with ScannerBit, the GAMBIT scanning module*, *Eur. Phys. J. C* **77** (2017) 761, [arXiv:1705.07959].

[7] GAMBIT Collaboration: P. Athron, C. Balázs, *et. al.*, *Global fits of GUT-scale SUSY models with GAMBIT*, *Eur. Phys. J. C* **77** (2017) 824, [arXiv:1705.07935].

[8] GAMBIT Collaboration: P. Athron, C. Balázs, *et. al.*, *A global fit of the MSSM with GAMBIT*, *Eur. Phys. J. C* **77** (2017) 879, [arXiv:1705.07917].

[9] GAMBIT Collaboration: P. Athron *et. al.*, *Combined collider constraints on neutralinos and charginos*, *Eur. Phys. J. C* **79** (2019) 395, [arXiv:1809.02097].

[10] B. Farmer, for the GAMBIT Collaboration, *Status of supersymmetric models with GAMBIT*, in *these proceedings*

[11] S. Hoof, F. Kahlhoefer, P. Scott, C. Weniger, and M. White, *Axion global fits with Peccei-Quinn symmetry breaking before inflation using GAMBIT*, *JHEP* **03** (2019) 191, [arXiv:1810.07192].

[12] GAMBIT Collaboration: P. Athron, C. Balázs, *et. al.*, *Status of the scalar singlet dark matter model*, *Eur. Phys. J. C* **77** (2017) 568, [arXiv:1705.07931].

[13] P. Athron, J. M. Cornell, *et. al.*, *Impact of vacuum stability, perturbativity and XENON1T on global fits of $\mathbb{Z}_2$ and $\mathbb{Z}_3$ scalar singlet dark matter*, *Eur. Phys. J. C* **78** (2018) 830, [arXiv:1806.11281].

[14] GAMBIT Collaboration: P. Athron *et. al.*, *Global analyses of Higgs portal singlet dark matter models using GAMBIT*, *Eur. Phys. J. C* **79** (2019) 38, [arXiv:1808.10465].

[15] XENON: E. Aprile *et. al.*, *First Dark Matter Search Results from the XENON1T Experiment*, *Phys. Rev. Lett.* **119** (2017) 181301, [arXiv:1705.06655].

[16] XENON: E. Aprile *et. al.*, *Dark Matter Search Results from a One Ton-Year Exposure of XENON1T*, *Phys. Rev. Lett.* **121** (2018) 111302, [arXiv:1805.12562].

PoS(ALPS2019)027